Thermal modeling of the infrared reflow process for Solder Ball Connect (SBC)

by H. V. Mahaney

A thermal model of the infrared reflow process has been developed for an FR-4 card populated with an array of Solder Ball Connect (SBC) modules. The analysis of the three-dimensional, transient, finite element model accounts for radiative exchange within the infrared oven and for the heat conduction (nonisotropic) within the modules and card. Transient temperature profiles of selected points and three-dimensional temperature distributions at selected times are presented to describe the primary heat-transport mechanisms. Numerical predictions and empirical data indicate that the SBC modules are relatively isothermal throughout the infrared reflow process. Therefore, every solder ball within the array exhibits a nearly identical thermal profile. This result is fortunate, since the inner solder ball connections cannot be visually inspected. The influence of module spacing and the ability to improve the reflow process by use of a high-emissivity cap coating are demonstrated.

Introduction

Solder Ball Connect (SBC) is an area array surface mount technology (SMT) in which a ceramic substrate containing one or more chips (a "module") is connected to an FR-4 card by the use of an array of high-temperature-melting 90%Pb/10%Sn solder balls and eutectic solder [1]. Interconnection between the card and the SBC module (as well as other surface mount components, in general) is typically accomplished with an infrared (IR) reflow process. In this process, a printed circuit card with solder paste applied to its pads and with modules placed thereon is passed through an infrared reflow oven. The primary purpose of this reflow process is to melt the solder paste, wet the surfaces to be connected, and solidify the solder into a strong metallurgical bond [2]. The reliability of this bond is inherently dependent upon the thermal profile the bond experiences throughout the IR reflow process.

A radiation-dominated IR reflow oven is shown schematically in **Figure 1**. Since the oven is nearly 100 times as long as the spacing between the top and bottom heater panels, Figure 1 is not drawn to scale. A conveyor belt, moving at constant velocity, is employed to transport the card populated with modules through the oven. Forty

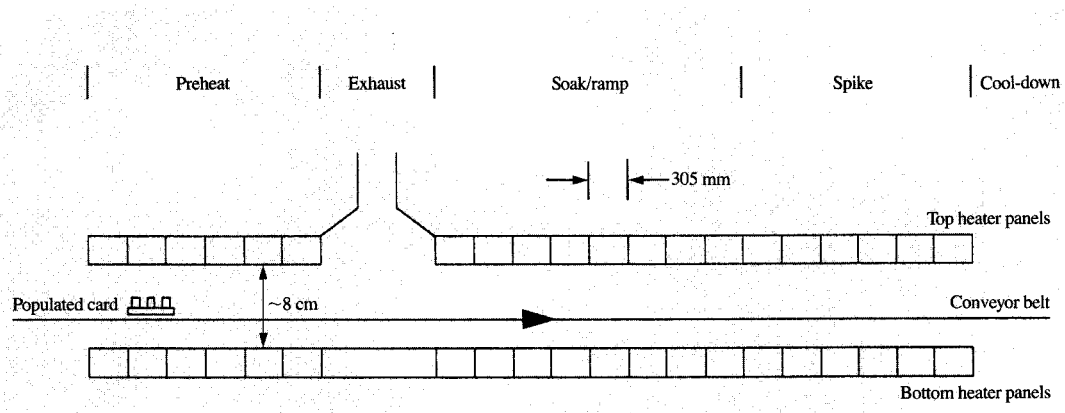

Figure 1

Schematic of infrared reflow oven.

heater panels, half above and half below the conveyor belt, are individually set to specified temperatures and used to heat the card and modules. These heater panels employ the secondary-emission principle, in which an imbedded resistive element heats a flat surface which in turn is the radiant source [3].

A typical oven profile consists of an initial preheating region, an exhaust section, a long soak/ramp region, and a final spike region. The initial preheat region provides a period of rapid heating that allows fast processing without overstressing components. To remove the paste volatiles from the system, air is drawn into the oven from both ends and is forced out of the system via the exhaust stack. The soak/ramp region is characterized by slower heating, allowing the temperature differentials within the assembly, which are created by the preheat section, to decrease, and bringing the entire assembly to a more or less uniform temperature just below the eutectic temperature. In the spike region, the temperature of the solder is raised above the eutectic solder reflow temperature (183°C) for 30 to 60 seconds, in order that the solder completely wet the solder joint.

Previous thermal modeling of the IR reflow process is limited to a few studies. Glaser and Juaire [4] performed a two-dimensional finite element thermal-conduction analysis of a representative cross section of a typical plastic leaded chip carrier undergoing an IR reflow process. However, time-dependent data from experimental measurements were used to define the thermal boundary conditions in the model; therefore, the radiative and convective transport within the oven was not directly simulated. Guided by the work of Fernandes et al. [5], Eftychiou et al. [6] employed a hierarchical modeling approach to estimate the thermal response of a card assembly undergoing an IR reflow process. In the latter study, a "tunnel model" that employed convective correlations was used to estimate thermal conditions within the oven, while a "card model" used the predictions of the tunnel model, in conjunction with a conductive and radiative heat transfer analysis, to estimate the detailed thermal response of the card. This two-dimensional analysis was applied to a series of J-leaded, plastic-encapsulated chip carriers mounted on an FR-4 circuit card that was processed in a relatively short oven of length 720 mm. Extensions of this model, which include the solution of the two-dimensional Navier–Stokes and energy equations, are given in [7] and [8]; they were applied, respectively, to an unpopulated card and a card populated with plastic-encapsulated surface mount modules. In both cases, the same short oven length (720 mm) was used. In these simulations [6–8], the thermal response of the card was shown to be radiation-dominated, while convective heating of the card occurred early in the reflow process and convective cooling occurred near the end of the process. Overall variations in the predicted solder temperature profile due to changes in convective heat transfer were modest, but the period during which the solder was molten was sensitive to the convective transport.

On the basis of the work cited above, which neglects convective transport within the oven, this paper discusses a thermal analysis of the IR reflow process for SBC modules being processed within an industrial-size furnace of length 7010 mm. The construction of the SBC assembly, however, is significantly different from that of the plastic-encapsulated chips considered above [4, 6, 8] in terms of module-to-card interconnection, dimensions, and thermal

properties (e.g., density, specific heat, thermal conductivity, and emissivity).

Numerical model

A thermal conduction analysis, with imposed radiative boundary conditions, was performed using the general-purpose finite element programs CAEDS® [9] and ANSYS® [10] to simulate the IR reflow process for SBC. Both radiative and convective boundary conditions were applied in the subsequent cool-down process. The three-dimensional, transient, nonisotropic heat-conduction equation solved in this analysis may be expressed as

$$\rho c_p\left(\frac{\partial T}{\partial t}\right) = \frac{\partial}{\partial x}\left(k_{xx}\frac{\partial T}{\partial x}\right) + \frac{\partial}{\partial y}\left(k_{yy}\frac{\partial T}{\partial y}\right) + \frac{\partial}{\partial z}\left(k_{zz}\frac{\partial T}{\partial z}\right) + q.$$

(The symbols are defined in the Appendix.) This equation is solved by an implicit direct integration scheme based on a modified Houbolt method employing a quadratic temperature function [10].

By assuming an infinite array of evenly spaced square SBC modules, as shown in **Figure 2**, the computational domain can be reduced via geometric symmetry arguments to one eighth of an SBC module and associated card (shown shaded in Figure 2). This symmetry argument does not strictly hold for the radiative boundary condition, since one row of modules will enter a given location in the oven just before or just after the adjacent rows of modules. Hence, heat conduction to or from different rows of SBC modules on the card is not included in this analysis.

The finite element representation of a 32-mm-square SBC module with a module-to-module spacing of $S = 5$ mm is shown in **Figure 3**. The thermal analysis considers heat transport by diffusion in each of the system components, which include FR-4 card, solder ball array, ceramic substrate, epoxy bond, C-4 (controlled collapse chip connection) array/air layer, chip, thermal grease, air, and aluminum cap. The epoxy bond layer, which attaches the aluminum cap to the substrate, and the C-4 array/air layer, which attaches the chip to the substrate, are very thin and are not apparent in Figure 3. Of the system components, the FR-4 card, solder ball array, and C-4 array/air layer are actually composites of several materials. The 2.3-mm-thick (0.090-in.) FR-4 card contains four 0.035-mm-thick (0.0014-in.) copper planes, and a plated through via is associated with each solder ball. Each via is modeled, allowing distinct thermophysical properties to be associated with each region of the card, depending on whether or not it contains a plated through via. The effective in-plane (k_{xx}, k_{yy}) and through-plane (k_{zz}) thermal conductivities of the FR-4 card were respectively derived from parallel and series combinations of thermal resistances of the individual layers of the card. The internal power planes substantially increase the in-plane thermal conductivity over that of pure FR-4 ($k = 0.2$ W/mK), but provide little increase of the through-plane conductivity. In contrast, the plated via substantially increases the through-plane conductivity for the via locations, but has little effect on the overall in-plane conductivity. The solder balls are the only system component whose geometric shape is not directly simulated in the model. A separate micro finite element model [11] of a single solder ball interconnection, which captured the three-dimensional spherical shape of a 90%Pb/10%Sn solder ball, eutectic solder, and pad interconnections, was used to predict the effective thermal resistance. The thermophysical properties of the two solid brick elements that define each solder ball in the IR reflow model were specified so as to yield this effective thermal resistance. Weighted thermophysical properties were also employed for the C-4/air layer. The density × specific-heat product (ρc_p) for the three composite components was similarly computed so that the total thermal mass was accounted for. All thermophysical properties [12–17] employed in the model, based upon the weighting

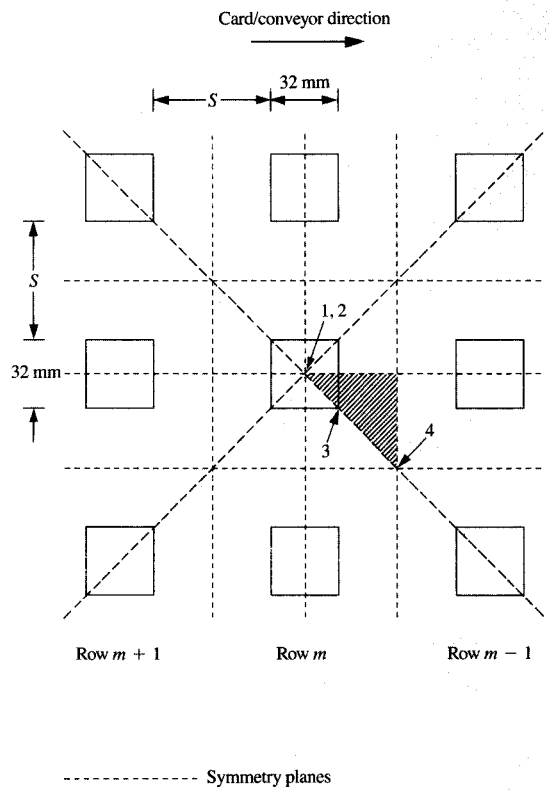

Figure 2

Numerical and experimental geometric array configuration, showing the computational domain (shaded) and the thermocouple locations (1–4).

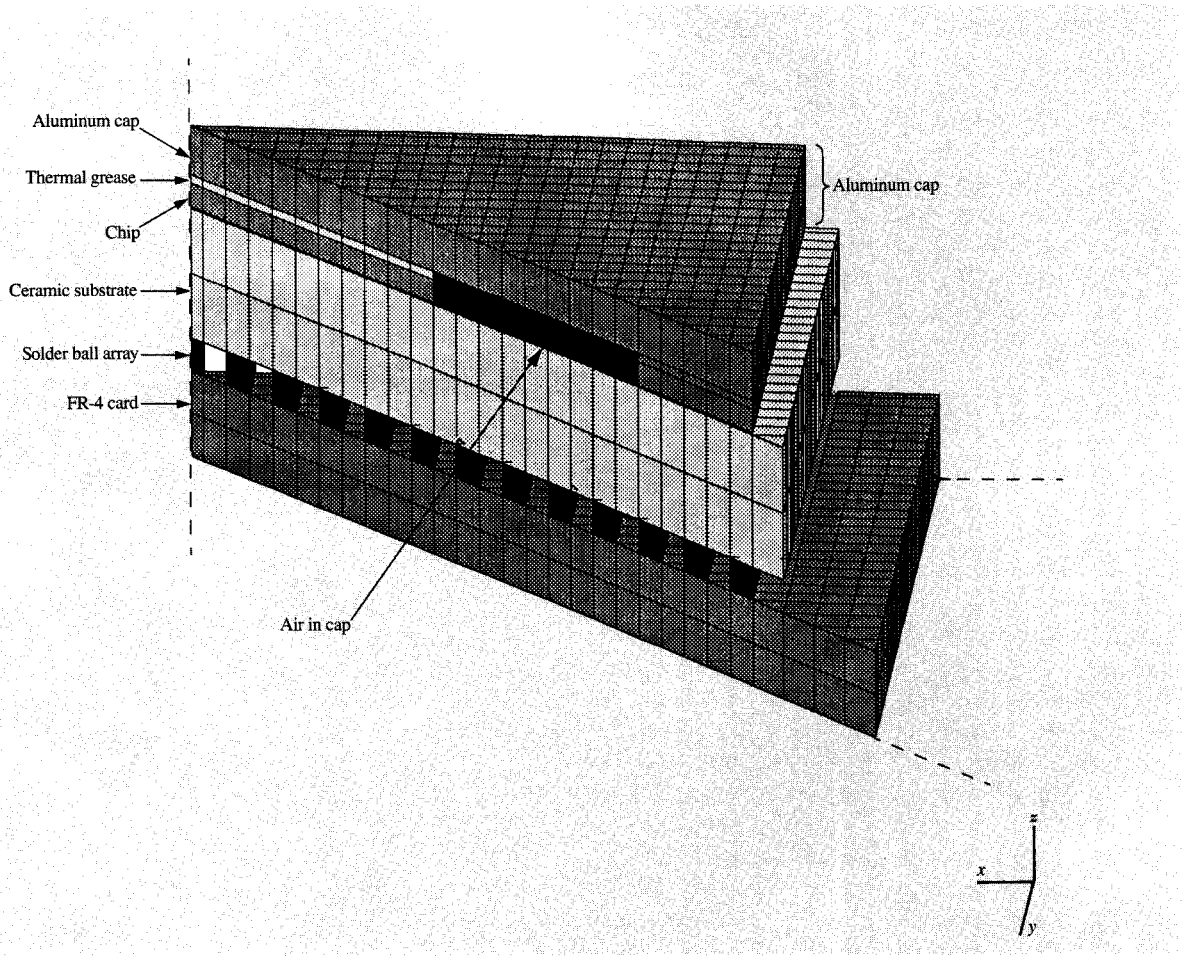

Figure 3

Finite element representation of one eighth of a 32-mm-square SBC module and neighboring card area, with module-to-module spacing of 5 mm.

procedures described above, are listed in **Table 1**. Temperature-dependent properties are given in **Table 2**.

During the IR reflow process, the temperature difference between the oven heater panels and the populated card is relatively large and is the predominant differential for the entire heating process, while the temperature differences between the card and the individual SBC modules are relatively small. Thus, the radiative exchange between the oven heater panels and the populated card is considered in the analysis, while that between the card and the individual components is not.

As the populated card travels through the oven, the radiative conditions experienced by the card continually change. Because the size of the heater panel is significantly greater than that of the module, a module and card at the center of a heater panel essentially participate in radiative exchange only with the heater panel directly above and the one directly below. However, as a module and card approach the end of these heater panels, they begin to participate in radiative exchange with the adjacent pair of heater panels as well. Accordingly, the radiative conditions experienced by the module and card do not undergo sudden step changes, but encounter smooth transitions from one region in the oven to the next.

Modeling this time-dependent radiative exchange may be accomplished in at least two ways. With one approach, the radiative exchange between the populated card and three pairs of panel heaters (upstream, current, downstream) may be considered. Utilization of this technique requires that a) view factors between each surface element of the model and all three pairs of heater panels be computed as a function of time (i.e., as a function of the relative position of the card and the heater panels), and b) three radiation links be created and solved for every surface

Table 1 Thermophysical properties of materials used in model.

Material	*Density* ρ (kg/m^3)	*Specific heat* c_p (J/kgK)	*Thermal conductivity* k_{xx} *and* k_{yy} (W/mK)	*Thermal conductivity* k_{zz} (W/mK)
FR-4 and power planes	1800	1570	27.2	0.215
FR-4 and vias	1800	1570	22.3	25.6
Solder ball	10500	167	48.6	48.6
Ceramic substrate	3800	780	*	*
Epoxy bond	1230	1900	0.5	0.5
C-4/air layer	1380	200	4.7	4.7
Chip	2330	*	*	*
Thermal grease	3250	730	1.15	1.15
Air	0.77	1021	0.037	0.037
Aluminum cap	2702	*	200	200

*See Table 2.

Table 2 Temperature-dependent properties of materials used in model.

Material	*Property*	*25°C*	*125°C*	*225°C*	*325°C*
Ceramic substrate	Thermal conductivity k_{xx}, k_{yy}, k_{zz} (W/mK)	17.6	11.6	11.6	11.6
Chip	Thermal conductivity k_{xx}, k_{yy}, k_{zz} (W/mK)	148	98.9	80.4	61.9
Chip	Specific heat c_p (J/kgK)	712	790	829	867
Aluminum cap	Specific heat c_p (J/kgK)	903	949	991	1033

element that participates in the radiative exchange. With a second approach, the card may be assumed to participate in radiative exchange with a single pair of heater panels whose temperatures are linearly ramped from time step to time step, depending upon the position of the card with respect to the heater panels. The latter technique has the advantages that since the view factors are independent of time, they need be calculated only once, and that the number of radiative links needed for the analysis is one third of that required for the former approach, thus significantly decreasing the CPU time required for the solution. This latter option was employed, and the time step, t_s, was set to one third of the time necessary for a module to travel the length of a heater panel: $t_s = L_p/3V$, where L_p is the heater panel length and V is the constant conveyor belt velocity. As a result of this ramping process, the oven panel temperature employed in the simulation is linearly ramped from $T_{\text{panel},\,n}$, the temperature of heater panel n, to $T_{\text{panel},\,n+1}$, the temperature of heater panel $n + 1$, in three steps and simulates the smooth transition from one heater panel to the next.

Thermal transport within the exhaust region of the oven is modeled by assuming that the radiative exchange occurs between the populated card and the exhaust flue (which is at 150°C because of convective heat transfer with the exhaust air).

The radiation model assumes diffuse gray behavior*; therefore, the net radiative transfer between the reflow environment (i.e., heater panels, exhaust, and surroundings) and each surface element of the model that participates in the radiative exchange may be expressed as

$$Q = \sigma \varepsilon F A (T_{\text{env}}^4 - T^4),$$

where Q is the heat flow rate; σ is the Stefan–Boltzmann constant; ε is the emissivity; F is the view factor; A is the exposed surface area of the finite element; T is its surface temperature; and, as shown in **Figure 4**, T_{env} is the temperature of the reflow environment, which comprises the oven (heater panels and exhaust) and the surroundings associated with the cool-down process. In this study, the top and bottom heater panels at each location were set to the same temperature.

Emissivity values used in the analysis are given in **Table 3**. The emissivity values for the FR-4 card and aluminum cap were measured using an infrared radiometric microscope. The emissivity of the aluminum cap was found to be sensitive to the surface finish/oxidization and to decrease with increasing temperature; the emissivity employed

*A gray surface is one for which the spectral emissivity and absorptivity are independent of wavelength over the spectral regions of the surface irradiation and emission. A diffuse surface is one for which the intensity associated with the incident, reflected, and emitted radiation is independent of direction.

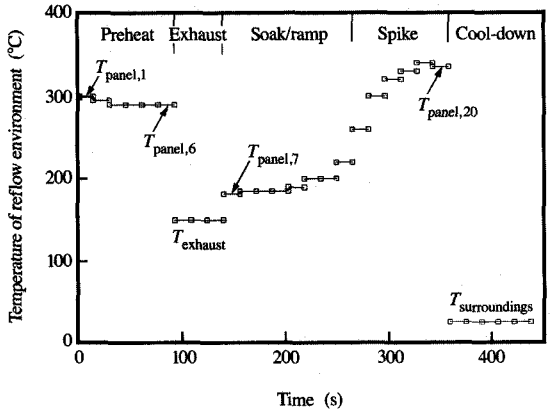

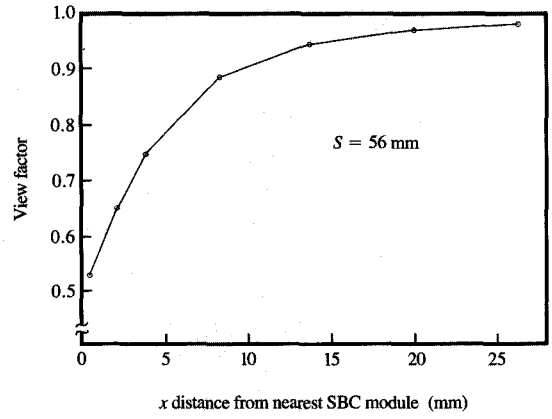

Figure 4

Temperature of the reflow environment, which comprises heater panels, exhaust, and surroundings.

Figure 5

View factor for the top surface of the card as a function of the x distance from the nearest SBC module.

Table 3 Emissivity values used in model.

Material	ε
FR-4	0.9
Aluminum cap	0.2
Aluminum cap, anodized	1.0
Ceramic substrate	0.7

in the analysis was typical of the measured data. Uncertainties associated with the emissivity measurements were estimated to be 0.05. The emissivity value of the ceramic substrate was based on data found in the literature. More recent measurements, however, indicate that the actual emissivity may be ≥0.9. Nonetheless, model predictions are relatively insensitive to the substrate emissivity, since only the small surface area associated with the sides of the substrate participates in the radiative exchange.

The radiative exchange between the surface elements of the model and the oven heater panels corresponds to surfaces that are either offset parallel or offset perpendicular. View factors for the model were computed as a function of position using view factor algebra and the analytical results presented by Siegel and Howell [18]. View factors for the bottom of the card and the top of the cap were unity, while those for the top of the card and the sides of the cap and substrate were less than unity because of shading effects. The computed view factor for the top surface of the card is given in **Figure 5** (for module-to-module spacing = 56 mm) as a function of the x distance from the nearest SBC module. As the distance from the SBC module increases, the effect of shading diminishes, so that the view factor approaches unity asymptotically. On the other hand, for regions close to the SBC module, the effect of shading is significant and the view factor is near 0.5. The computed view factor for the side surfaces is 0.47.

The IR oven under consideration in this study is radiation-dominated, so convective heat transfer within the oven is not considered. This assumption is more appropriate for the preheat section of the oven, where the entering air and card are at room temperature (25°C) and there is no temperature difference between the air and card to cause convective heat transfer. In contrast, at the exit of the oven, unheated air is drawn into the oven over the heated card, and convective cooling of the card occurs. Incorporation of convective heat transfer within the modeling framework presented herein would be straightforward, but would require the nontrivial specification of convective heat transfer coefficients and bulk air temperatures as functions of position within the oven. Obtaining such information would have required a full computational fluid dynamics simulation of the oven, which was beyond the scope of this study. Multimode cooling of the card occurs after it exits the oven, where natural convective cooling enhances the radiative transport to the cool surroundings. On the basis of natural convective correlations for heat transfer from a horizontal surface [12], a heat transfer coefficient of 10 W/m^2°C was assumed for the cool-down process.

Experimental methods

An FR-4 card populated with an array of 32-mm-square SBC modules with a module-to-module spacing S of approximately 56 mm was instrumented with four type-K thermocouples. These were attached with epoxy to 1) the center, top surface of the aluminum cap, 2) the center solder ball of the array, 3) one of the four corner solder balls of the array, and 4) a point on the card that is equidistant from the center of the module and the center of the diagonally located adjacent module. The x–y locations of these thermocouples are shown in Figure 2. Transient temperature data were measured and stored using a Multichannel Occurrent Logger Evaluator (Electronic Controls Design). We estimated uncertainty associated with the temperature measurements to be 1°C.

Results

Experimental measurements of the temperature response of a populated card that moved through the IR oven at a speed of 1.95 cm/s (46 in./min) are shown in **Figure 6.** Because of the low thermal mass per unit area of the card, as well as its high emissivity, the card far from the module (point 4 in Figure 2) heats up significantly faster than does the module, in the preheat section of the oven. In the exhaust and soak/ramp regions, the temperature differential between the card and module decreases, because of the lower exhaust and heater panel temperatures (Figure 4) and because of the conduction of heat from the card to the module. In the spike region, the card far from the module again heats up significantly faster than the module. Although the temperature of the card is higher than that of the module at the beginning of the cool-down region, the thermal energy per unit area of the card is significantly less than that of the module. Because of this and the high emissivity of the card, the card initially experiences a much steeper cooling curve than the module, so that shortly after cool-down begins, a temperature inversion is expected in which the card far from the module will be cooler than the module, and heat flow via conduction will proceed from the module to the card.

During the IR reflow process, temperature differentials within the SBC modules are small. The temperature response of the center of the top surface of the aluminum cap is seen to be nearly identical (within 5°C) to that of the center solder ball directly beneath the cap measurement point. Since a small but finite time is required for the heat to be conducted from the edge of the module to the center, the corner solder ball heats up slightly before the center solder ball. Because of the temperature inversion described above, the corner solder ball is also expected to cool down before the center solder ball. Although the temperature response of the center solder ball is slightly staggered in time as compared to that of the corner solder ball, Figure 6 indicates that the overall temperature profile and the maximum temperature experienced are nearly the same for the corner and center solder balls. Thus, all of the solder balls experience nearly identical temperature profiles and maximum temperature. Since area array attach components do not lend themselves to visual inspection of any connections other than those at the periphery, it is desirable that all of the connections have nearly identical

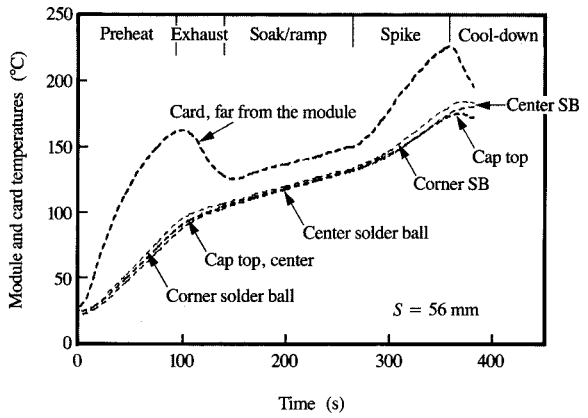

Figure 6

Measured temperature profile for a card with 32-mm-square SBC modules and a module-to-module spacing of 56 mm.

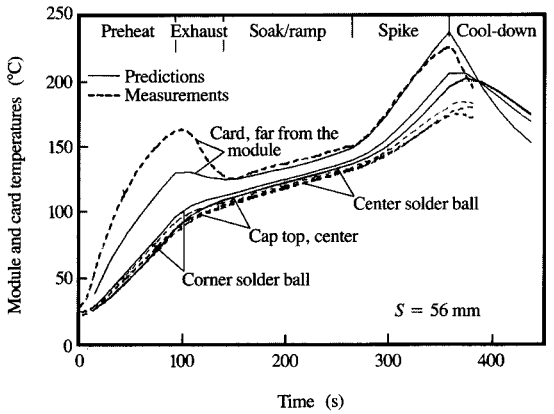

Figure 7

Comparison of measured and numerically predicted temperature profiles for a card with 32-mm-square SBC modules and a module-to-module spacing of 56 mm.

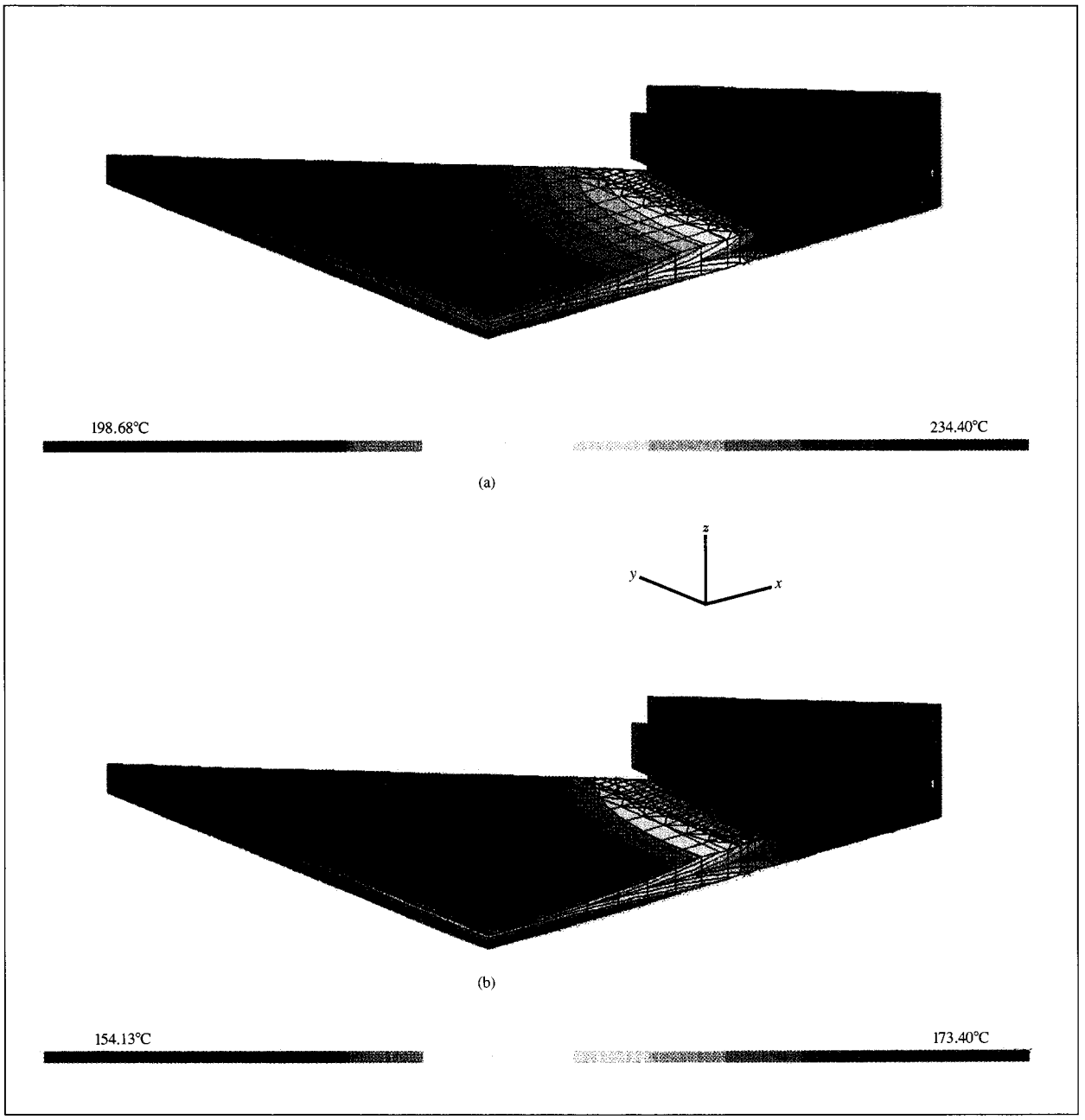

Figure 8

Three-dimensional temperature distribution for card and SBC module when the module is (a) at the end of the spike region (t = 360 s) and (b) at the end of the cool-down simulation (t = 438 s). For plot (a), the temperature differential between neighboring isotherms is 3.25°C; for plot (b), it is 1.75°C.

thermal profiles. This is because the absence of visible failures among the solder ball connections on the periphery provides some confidence that the remaining solder ball connections are satisfactory.

In **Figure 7**, numerical predictions for this IR reflow process are compared with the experimental results of Figure 6. Numerical predictions of the temperature of the card surface far from the module are significantly lower than the measured temperatures in the preheat and exhaust sections, but are in excellent agreement during the soak/ramp, spike, and cool-down regions (within 12°C). Numerical predictions for all measured positions on the

module are in excellent agreement with the measured data in the preheat, exhaust, and soak/ramp regions (within 6°C), but exceed the measured temperatures in the spike region. This discrepancy is attributed to convective cooling within the oven due to the inflow of unheated air at the oven exit, which is not included in the current analysis. The following trends described above for the experimental data are also evident in the numerical predictions: a) the widening temperature difference between the card far from the SBC module and the module itself in the preheat and spike regions, with a diminishing difference in the exhaust and soak/ramp regions, b) minimal temperature difference throughout the thickness of the SBC module, c) the corner solder ball heating up and cooling down just before the center solder ball, and d) a temperature inversion for all measurements.

The predicted temperature distribution of the card and module when the module is located at the end of the spike region (t = 360 s) is shown in **Figure 8(a)**. As described above, the low thermal mass per unit area of the card and the high card emissivity result in the card temperature significantly exceeding that of the module. The heat received by the card via radiative exchange with the oven is conducted along the card to the relatively cool module. Because of the excellent thermal conductivity values for the bulk of the SBC module, the SBC module is nearly isothermal. Temperature distributions for t < 360 s are qualitatively similar to those of Figure 8(a), but the temperature ranges correspond to those shown in Figure 7.

The predicted temperature distribution at the end of the cool-down simulation (t = 438 s) is shown in **Figure 8(b)**. Because of the low thermal mass per unit area and the high emissivity of the card, the card cools faster than the SBC module, and at this point in the cool-down process, the card is cooler than the module. Consequently, the SBC module is being cooled by radiative and convective heat transfer to the environment, as well as by conduction along the card.

To investigate the significance of conduction within the card to the heating and cooling process of the module, the analysis described above was repeated for a geometric configuration in which the spacing between SBC modules was decreased from 56 mm (Figures 5–8) to 5 mm (Figure 3), which, because of manufacturing and implementation restrictions, is the minimum allowable component spacing. All other simulation parameters, including the oven heater panel temperatures, view factors, and conveyor belt speed, are the same for the two simulations. Therefore, the radiative environment experienced by the SBC module is exactly the same for the two cases, and any difference between the resultant temperature responses of the module is due solely to differences in the amount of heat radiated from the oven heater panels to the card and subsequently conducted through the card to the module.

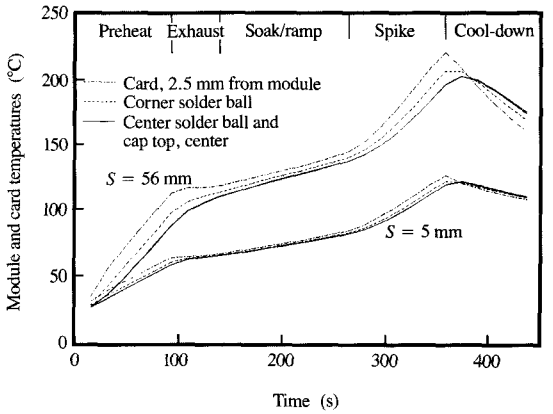

Figure 9

Numerical predictions of the temperature profile for two different values of component spacing.

The temperature responses of selected points are shown in **Figure 9** for the two module spacings. Decreasing the spacing drastically lowers the overall temperature profile for the module, causing the maximum temperature of the center solder ball to drop from 202°C to 121°C. The temperature for the larger-spacing case is significantly higher than for the small-spacing case because of the greatly increased card surface area, which results in more heat being radiated from the IR panels to the card and subsequently conducted from the card to the module. It should be noted that the connection between the card and module created by the solder ball array has low thermal resistance and does not inhibit this heat transfer. Thus, heat conduction through the card to the SBC module can be a significant mode of heat transfer, the importance of which is a strong function of module spacing and copper content of the card.

The SBC module heats up more slowly than the card, not only because of the higher thermal mass of the module, but because of the lower emissivity of the module cap (see Table 3). Thus, the radiative transport to the module can be enhanced by coating the aluminum cap with a high-emissivity coating. **Figure 10** indicates the predicted temperature response (with module separation of 56 mm) for cap emissivity values of 0.2 and 1.0. Increasing the cap emissivity enhances the radiative transport to the module and, as a result, increases the maximum temperature of the center solder ball (the one that heats up most slowly) by 11°C, and increases the dwell time above the eutectic temperature (183°C) by 20 seconds. Because of the higher module temperature, less energy is conducted through the

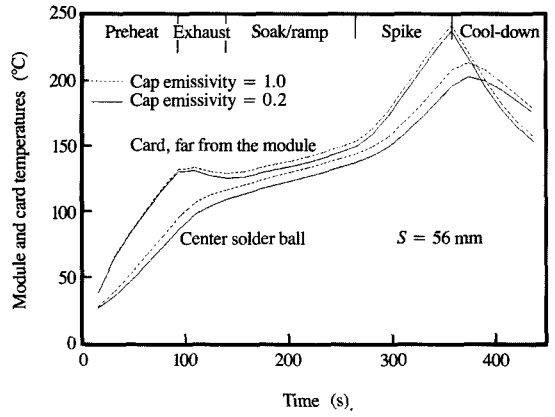

Figure 10

Numerical predictions of the temperature profile for two different values of cap emissivity.

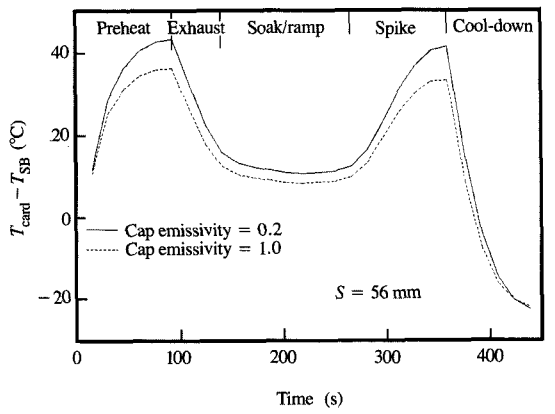

Figure 11

Numerical predictions of the temperature difference between the card far from the module and the center solder ball for two different values of cap emissivity.

card to the module, causing the card temperature to increase, although to a smaller degree than the module temperature.

The temperature difference between the card far from the module and the center solder ball is shown in **Figure 11**. The maximum temperature of the card occurs at the end of the spike region. For a cap emissivity of 0.2, the card temperature exceeds that of the center solder ball by up to 41°C, but this temperature difference can be reduced by 8°C (19%) for a cap with a high-emissivity coating. Since a successful reflow requires that the solder temperature be above the eutectic temperature for 30–60 seconds, yet that the card temperature not exceed a specified maximum value, minimization of this temperature difference yields improved reflow performance.

A subsequent experimental investigation of the temperature response of 32-mm-square SBC modules was conducted to verify the predicted influence of cap emissivity. Anodizing the cap resulted in the emissivity ε increasing from ~0.2 to >0.9. Although the measurements were performed using a thinner card (1.83 mm) and different oven temperatures than were employed in the work described above, results indicated that cap anodization increased the peak temperatures of the solder balls by 9 to 14°C and increased dwell time above the eutectic temperature by 25 to 37 seconds. Thus, these empirical data confirm the numerically predicted trends.

Conclusions

A finite element analysis and supporting empirical verification of the temperature response of an FR-4 card populated with an array of SBC modules during the IR reflow process has been conducted. Because of the low thermal mass per unit area and the high emissivity of the FR-4 card, the card far from the module heats up and cools down significantly faster than the module. Since the solder ball array provides a relatively low thermal resistance interconnection between the card and module, the card can be an important path for heat conduction into and out of the module. The significance of this path is highly dependent on module spacing and copper content in the card.

During the IR reflow process, temperature differentials within an SBC module are small; thus, all of the solder balls experience a similar thermal profile. Since area array components do not lend themselves to visual inspection of any of the connections other than the outermost row, this characteristic is highly desirable.

Numerical predictions and empirical data indicate that increasing the module-cap emissivity increases the peak temperature of the solder balls and their dwell time above the eutectic, yet it has a smaller effect on the temperature of the card. In this manner, the temperature differential between the relatively hot card and the cool module can be decreased, resulting in an improved reflow process.

Appendix: Symbols

c_p	specific heat
k	thermal conductivity
q	volumetric heat flow rate
S	module-to-module spacing
t	time
T	temperature
x, y, z	spatial coordinates
ε	emissivity
ρ	density

Acknowledgments

The author gratefully acknowledges the helpful interaction with and suggestions of Lawrence Buller, as well as the empirical acquisition of the nonanodized versus anodized temperature data by Donald Banks.

References

1. M. D. Ries, D. R. Banks, D. P. Watson, and K. G. Hoebener, "Attachment of Solder Ball Connect (SBC) Packages to Circuit Cards," *IBM J. Res. Develop.* **37**, 597–608 (1993, this issue).
2. C. L. Hutchins, "Optimization of Vapor Phase and Infrared Solder Reflow Processes," *Proceedings of the National Electronic Packaging and Production Conference*, Anaheim, CA, February 1987, pp. 516–524.
3. P. Zarrow, "Panel/Convection IR Reflow," *Circuits Manuf.* **28**, 47–49 (May 1988).
4. J. C. Glaser and M. P. Juaire, "Thermal and Structural Analysis of a PLCC Device for Surface Mount Processes," *Trans. ASME, J. Electron. Packaging* **111**, 172–178 (1989).
5. N. J. Fernandes, T. L. Bergman, and G. Y. Masada, "Thermal Effects During Infrared Solder Reflow—I. Heat Transfer Mechanisms," *Trans. ASME, J. Electron. Packaging* **114**, 41–47 (1992).
6. M. A. Eftychiou, T. L. Bergman, and G. Y. Masada, "Thermal Effects During Infrared Solder Reflow—II. A Model of the Reflow Process," *Trans. ASME, J. Electron. Packaging* **114**, 48–54 (1992).
7. T. L. Bergman, M. A. Eftychiou, and G. Y. Masada, "Thermal Processing of Discrete, Conveyorized Material," *Proceedings of the Winter Annual Meeting of the American Society of Mechanical Engineers* **HTD-224**, 27–34 (1992).
8. M. A. Eftychiou, T. L. Bergman, and G. Y. Masada, "A Detailed Thermal Model of the Infrared Reflow Soldering Process," *Trans. ASME, J. Electron. Packaging* **115**, 55–62 (1993).
9. *CAEDS Graphics Finite Element Modeler User's Guide*, Version 3, Release 1, IBM Corporation, 1988.
10. *ANSYS Engineering Analysis System User's Guide*, Revision 4.3, Swanson Analysis Systems, Inc., Houston, PA, 1987.
11. J. S. Corbin, "Finite Element Analysis for Solder Ball Connect (SBC) Structural Design Optimization," *IBM J. Res. Develop.* **37**, 585–596 (1993, this issue).
12. F. P. Incropera and D. P. DeWitt, *Fundamentals of Heat and Mass Transfer*, Second Edition, John Wiley & Sons, Inc., New York, 1985.
13. *Electronics Materials Handbook*, Vol. 1, ASM International, Materials Park, OH, 1989.
14. *Materials Handbook for Hybrid Manufacturing*, J. A. King, Ed., Artech House, Boston, 1988.
15. *Materials Engineering, Materials Selector 1990*, Penton Publishing, Cleveland, OH, 1989.
16. *Microelectronics Packaging Handbook*, R. R. Tummala and E. J. Rymaszewski, Eds., Van Nostrand Reinhold, New York, 1989.
17. R. J. Klein Wassink, *Soldering in Electronics*, Electrochemical Publishers Limited, Ayr, Scotland, 1984.
18. Robert Siegel and John R. Howell, *Thermal Radiation Heat Transfer*, Appendix C, McGraw-Hill Book Co., Inc., New York, 1981.

Received December 10, 1992; accepted for publication February 9, 1993

H. Victor Mahaney *IBM Advanced Workstations and Systems Division, 11400 Burnet Road, Austin, Texas 78758 (MAHANEY at AUSVMV).* Dr. Mahaney received his B.S.M.E. degree in 1984 at the University of Missouri–Rolla, his M.S.M.E. degree in the field of numerical heat transfer in 1986 at Purdue University, and his Ph.D. degree in the field of electronics cooling at Purdue University in 1989. In 1990 he joined the IBM Systems Technology Division, where he conducted numerical modeling for emerging packaging and interconnection technologies. In 1991 he joined the Advanced Workstations and Systems Division of IBM Personal Systems, where he is currently performing computational fluid dynamic analyses to optimize the cooling for advanced workstations. Dr. Mahaney is a member of the American Society of Mechanical Engineers.